bioRxiv

Sequential membrane- and protein-bound organelles compartmentalize genomes during phage infection

Emily G. Armbruster[a], Jina Lee[a], Joshua Hutchings[a,b], Arica R. VanderWal[a,b], Eray Enustun[a], Benjamin A. Adler[c,d], Ann Aindow[a], Amar Deep[e], Zaida K. Rodriguez[a], Chase J. Morgan[a], Majid Ghassemian[f], Emeric Charles[d,g], Brady F. Cress[d], David F. Savage[c,d,g,h], Jennifer A. Doudna[c,d,g,h,i,j,k], Kit Pogliano[a], Kevin D. Corbett[a,e], Elizabeth Villa[a,b,*], Joe Pogliano[a,*]

[a]School of Biological Sciences, University of California San Diego, La Jolla, CA 92093, USA.
[b]Howard Hughes Medical Institute, University of California San Diego, La Jolla, CA 92093, USA.
[c]California Institute for Quantitative Biosciences (QB3), University of California, Berkeley, CA 94720, USA.
[d]Innovative Genomics Institute, University of California, Berkeley, CA 94720, USA.
[e]Department of Cellular and Molecular Medicine, University of California San Diego, La Jolla, CA 92093, USA.
[f]Biomolecular and Proteomics Mass Spectrometry Facility, University of California San Diego, La Jolla, CA 92093, USA.
[g]Department of Molecular and Cell Biology, University of California, Berkeley, CA 94720, USA.
[h]Howard Hughes Medical Institute, University of California, Berkeley, CA 94720, USA.
[i]Department of Chemistry, University of California, Berkeley, CA 94720, USA.
[j]Environmental Genomics and Systems Biology Division, Lawrence Berkeley National Laboratory, Berkeley, CA 94720, USA.
[k]MBIB Division, Lawrence Berkeley National Laboratory, Berkeley, CA 94720, USA.

*Correspondence to: EV: evilla@ucsd.edu, JP: jpogliano@ucsd.edu

Eukaryotic viruses assemble compartments required for genome replication, but no such organelles are known to be essential for prokaryotic viruses. Bacteriophages of the family *Chimalliviridae* sequester their genomes within a phage-generated organelle, the phage nucleus, which is enclosed by a lattice of viral protein ChmA. Using the dRfxCas13d-based knockdown system CRISPRi-ART, we show that ChmA is essential for the *E. coli* phage Goslar life cycle. Without ChmA, infections are arrested at an early stage in which the injected phage genome is enclosed in a membrane-bound vesicle capable of gene expression but not DNA replication. Not only do we demonstrate that the phage nucleus is essential for genome replication, but we also show that the *Chimalliviridae* early phage infection (EPI) vesicle is a transcriptionally active, phage-generated organelle.

Introduction

Diverse eukaryotic viruses require dedicated genome replication compartments to concentrate host- and virus-encoded replication machinery and shield their genomes from host defenses (1–3). These compartments can be assembled from host cell membranes or virally-encoded proteins, or formed via liquid-liquid phase separation. In contrast, no compartments are known to be required for genome replication of prokaryotic viruses. Bacteriophages of the recently described family *Chimalliviridae* are the only prokaryotic viruses known to assemble a compartment, the phage nucleus, within which their genomes replicate (4–6) (**Fig. 1A**). The phage nucleus protects the phage genomes from host defenses including DNA-targeting CRISPR/Cas systems and restriction enzymes, but whether it is intrinsically essential for genome replication has remained unclear (1, 7–9). The phage nucleus is enclosed by a continuous 2-D lattice composed primarily of the virally-encoded protein chimallin (ChmA) which gives *Chimalliviridae* its name (8, 10, 11). In a striking parallel to the subcellular organization orchestrated by the eukaryotic nucleus, this phage-generated organelle selectively imports DNA replication and transcription machinery and excludes metabolic enzymes and ribosomes in the bacterial cytoplasm. Here we applied a newly developed protein expression knockdown technology, CRISPRi-ART, to investigate whether the phage nucleus is essential for *Chimallivirus* genome replication.

CRISPRi-ART as a Genetics Tool for Nucleus-Forming Phages. While *Chimalliviridae* phages sequester their dsDNA genomes within the ChmA-based phage nucleus, rendering them inaccessible to traditional genome editing tools, viral mRNAs are exported to the cytoplasm to be translated by host ribosomes (4–6). Taking advantage of this vulnerability, we knocked down ChmA via CRISPRi-ART to determine how inhibiting phage nucleus assembly affects genome replication of *E. coli* phage Goslar. CRISPRi-ART (CRISPR interference by Antisense RNA Targeting) uses catalytically inactive *Ruminococcus flavefaciens* Cas13d (dRfxCas13d) to specifically suppress expression of proteins of interest (**Fig. 1B**) (12, 13). Guide-directed binding of targeted RNA triggers collateral RNAse trans-activity in wildtype Cas13, leading to death or dormancy of bacterial cells (14–17). However, mutation of key active site residues in dRfxCas13d's two HEPN (higher eukaryote and prokaryote nucleotide-binding) domains allows it to bind target RNA without inducing nuclease activity (12, 13, 18). Therefore, dRfxCas13d can be used to inhibit expression of a protein by binding and thereby occluding the translational start site of the corresponding mRNA (12, 13, 19). CRISPRi-ART has been shown to be highly effective as a genetics tool for diverse phages, including Goslar (12).

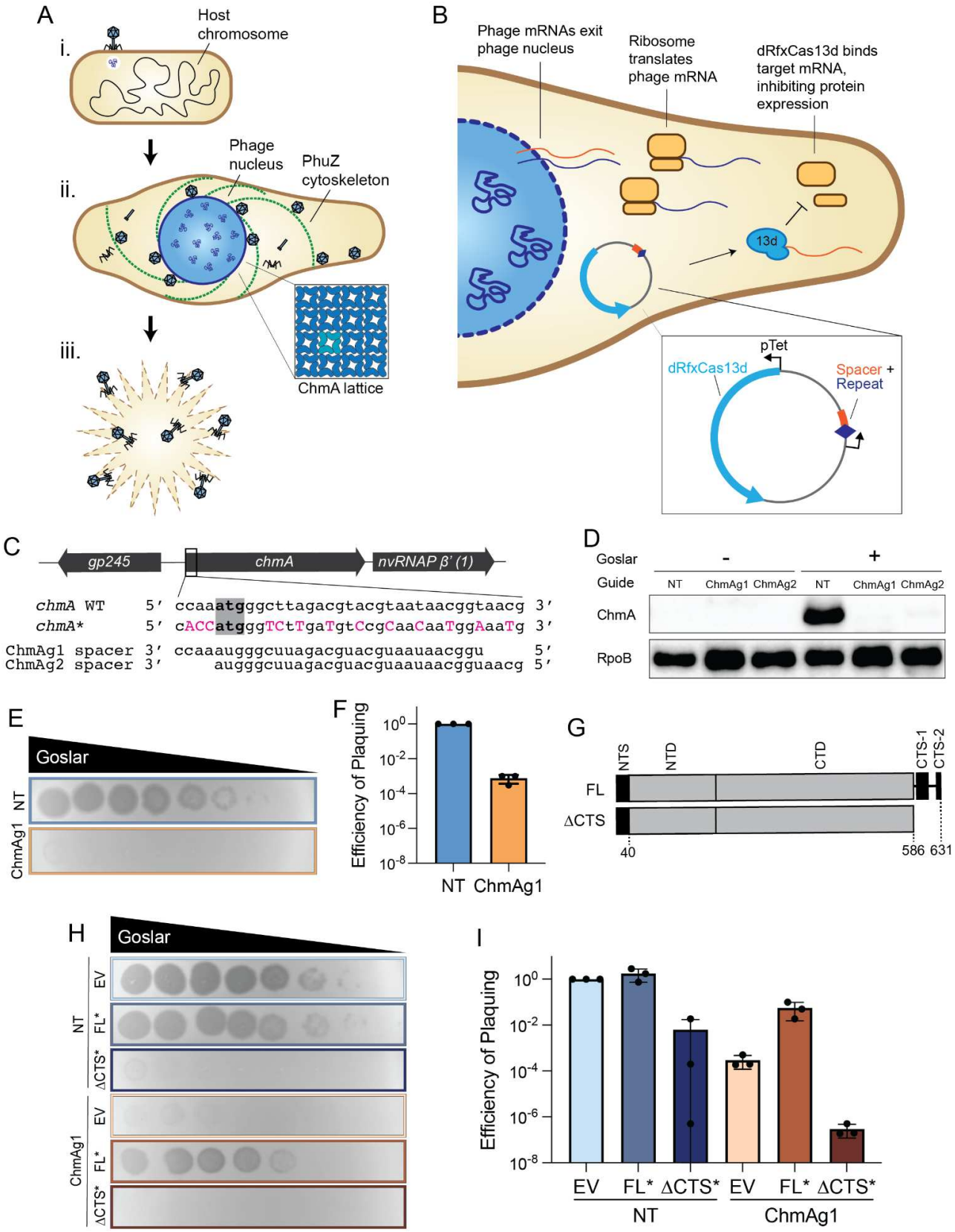

Figure 1 | ChmA knockdown inhibits Goslar reproduction. a, Goslar life cycle: i) phage attachment and genome injection, ii) phage nucleus growth and genome replication with inset of ChmA lattice in side-view (tetramer in cyan), iii) host cell lysis. **b**, Goslar protein expression knockdown via CRISPRi-ART. Viral mRNAs (orange and blue) are exported from the phage nucleus and proteins are expressed by host ribosomes. Expression of a protein of interest (orange) is inhibited by dRfxCas13d ("13d") programmed with crRNA binding the transcript's translational start site. dRfxCas13d and crRNA are expressed from one plasmid (inset). **c**, *chmA* target and crRNA sequences. The translational start site is in gray. Recoded nucleotides in *chmA** are capitalized in pink. **d**, Western blot of uninfected and Goslar-infected *E. coli* lysates expressing dRfxCas13d and either a non-targeting guide (NT), ChmAg1 or ChmAg2. RpoB (*E. coli* RNA polymerase β subunit) was used as a loading control. **e-f**, Efficiency of plaquing (EOP) assay comparing Goslar reproduction in the non-targeting and knockdown strains. **e**, Representative plate photos. **g**, Full-length ChmA (FL) and truncated ChmA (ΔCTS) domain diagram. **h-i**, EOP assay for complementation with either full-length ChmA* (FL*) or the truncated mutant (ΔCTS*). EV = empty vector. **h**, Representative plate photos.

Results

ChmA Knockdown Inhibits Goslar Reproduction. To characterize the effect of ChmA knockdown on Goslar reproduction, we confirmed the efficacy of two *chmA* transcript-targeting guides, ChmAg1 and ChmAg2 (**Fig. 1C**). We collected whole-cell lysates of Goslar-infected *E. coli* MC1000 strains coexpressing each guide with dRfxCas13d 90 minutes post infection (mpi) and determined ChmA expression levels via western blot (**Fig. 1C, Fig. S1**). Both guides dramatically reduced ChmA expression, but only ChmAg1 was used in our study as it consistently induced a slightly stronger knockdown.

Goslar's efficiency of plaquing (EOP) was reduced ~1,000-fold when infecting the host strain expressing dRfxCas13d and ChmAg1 ("knockdown strain") compared to the host strain expressing dRfxCas13d and a non-targeting guide ("non-targeting strain") (**Fig. 1E-F**), suggesting that ChmA is required for phage reproduction. Complementation by expression of ChmA from a *chmA* gene re-coded to avoid ChmAg1 targeting (*chmA**, **Fig. 1C**) restored the EOP ~200-fold (FL* for "full-length ChmA*", **Fig. 1G-I**). This demonstrated that inhibition of phage reproduction was caused by lack of ChmA and not due to off-target effects of dRfxCas13d.

We previously observed that deleting the C-terminal segments (CTS1 and CTS2) of *Pseudomonas chlororaphis* phage 201phi2-1 ChmA abolished self-assembly into oligomers *in vitro* (10). Therefore, to determine whether ChmA lattice assembly is required for Goslar reproduction, we investigated whether ChmA* lacking both C-terminal segments (ΔCTS*, **Fig. 1G**) could complement ChmA knockdown. Not only did ChmAΔCTS* fail to complement ChmA knockdown, but its expression reduced Goslar EOP by an additional 1000-fold (**Fig. 1H-I**). Notably, ChmAΔCTS* also acted as a dominant negative mutant, severely reducing Goslar EOP when expressed in the non-targeting strain and when expressed in the absence of the knockdown system (**Fig. 1H-I, Fig. S2**). Previous fluorescence microscopy studies have shown that eGFP-tagged C-terminal segment ChmA truncations associate with the wildtype ChmA lattice produced by 201phi2-1 during infection, indicating that they co-assemble with the full-length protein (10). This suggests that ChmAΔCTS*, untagged and expressed at a high concentration, likely poisons the lattice of phage-generated wildtype ChmA, preventing phage nucleus assembly.

Thus, two independent methods for inhibiting ChmA lattice assembly inhibit lytic phage growth. These results demonstrate that ChmA, and therefore the phage nucleus, is essential for Goslar's life cycle.

The ChmA Lattice is Required for Phage DNA Replication. We used single-cell fluorescence microscopy to determine the stage of infection at which Goslar's life cycle was inhibited by ChmA knockdown. At 90 mpi, infected non-targeting cells were swollen, elongated and contained large phage nuclei visible by brightfield microscopy and DAPI staining (**Fig. 2A, Fig. S3**). The host chromosomes of infected cells were also partially degraded. This phenotype is characteristic of Goslar infections (9), indicating that non-targeting CRISPRi-ART did not disrupt normal infection progression. Infected ChmAg1 knockdown cells were also significantly swollen and elongated at 90 mpi but almost none of them had developed mature phage nuclei. Instead, infected cells contained small DAPI-stained puncta surrounded by a zone devoid of host chromosomal DNA (**Fig. 2B, Fig. S3**). These DAPI-stained puncta appeared similar to the initially injected phage genomes previously observed early in the *Chimalliviridae* life cycle (9, 20). Therefore, to determine whether the DAPI-stained puncta were Goslar genomes arrested at an early stage of infection, we investigated whether sfGFP-ChmA colocalized with them. sfGFP-ChmA can be expressed in the knockdown strain because the target sequence is not at the translational start site of the fusion protein (12, 13). We expressed sfGFP-ChmA at a low concentration from a second plasmid to avoid complementation of ChmA knockdown. In non-targeting cells, sfGFP-ChmA formed a punctum that colocalized with the DAPI-stained punctum of initially injected phage DNA early during infection (10 mpi) and integrated into the ChmA lattice of the mature phage nuclei surrounding the phage DNA at later time points (45 and 90 mpi) (**Fig. 2D**). This recapitulated the previously observed pattern of GFP-tagged ChmA localization over the course of Goslar infection (9). In knockdown cells, sfGFP-ChmA co-localized with the DAPI-stained puncta (>80% co-localization, n = 106, 122, 122) throughout infection (10, 45 and 90 mpi) (**Fig. 2E**). sfGFP alone does not colocalize with the DAPI-stained puncta and is excluded from mature phage nuclei, remaining diffuse in the cytoplasm (**Fig. S4**).

By quantifying the cross-sectional area of DAPI-stained phage DNA as well as phage DNA quantity in terms of total DAPI intensity, we found that ChmA depletion severely inhibited both phage nucleus expansion and viral DNA replication (**Fig. 2F, H**). In fact, the area and DAPI intensity of phage DNA in the knockdown strain were comparable to that of Goslar particles outside of cells in the same microscopy fields (**Fig. 2C, G, I**), suggesting that intracellular DAPI-stained puncta contain only a single, non-replicating Goslar genome (**Fig. 2C**). In the knockdown strain, phage DNA area was >0.1 μm^2 in only 5.9% of infections (n = 171) compared to 0.0% for extracellular phage (n = 171, **Fig. 2G**) and 90.5% for non-targeting strain infections (n = 178, **Fig. 2F**). Similarly, the total DAPI intensity of phage DNA was >50 AU in 11.1% of infections in the knockdown strain (n = 171) versus 0.6% for extracellular phage (n = 171, **Fig. 2I**) and 97.8% for non-targeting strain infections (n = 178, **Fig. 2H**). Time-lapse brightfield microscopy revealed that arrested Goslar infections do not proceed even after 210 mpi (**Fig. 3A**). Unlike non-targeting strain infections (n = 248), for which the average time-to-lysis is ~160 minutes, infected knockdown strain cells remained intact (n = 271), often continuing to slowly grow in length (but not dividing or septating) up to at least 210 mpi without developing visible phage nuclei (Supplementary movies 1-2). Taken together, these data suggest that phage DNA is injected but fails to replicate during ChmA knockdown.

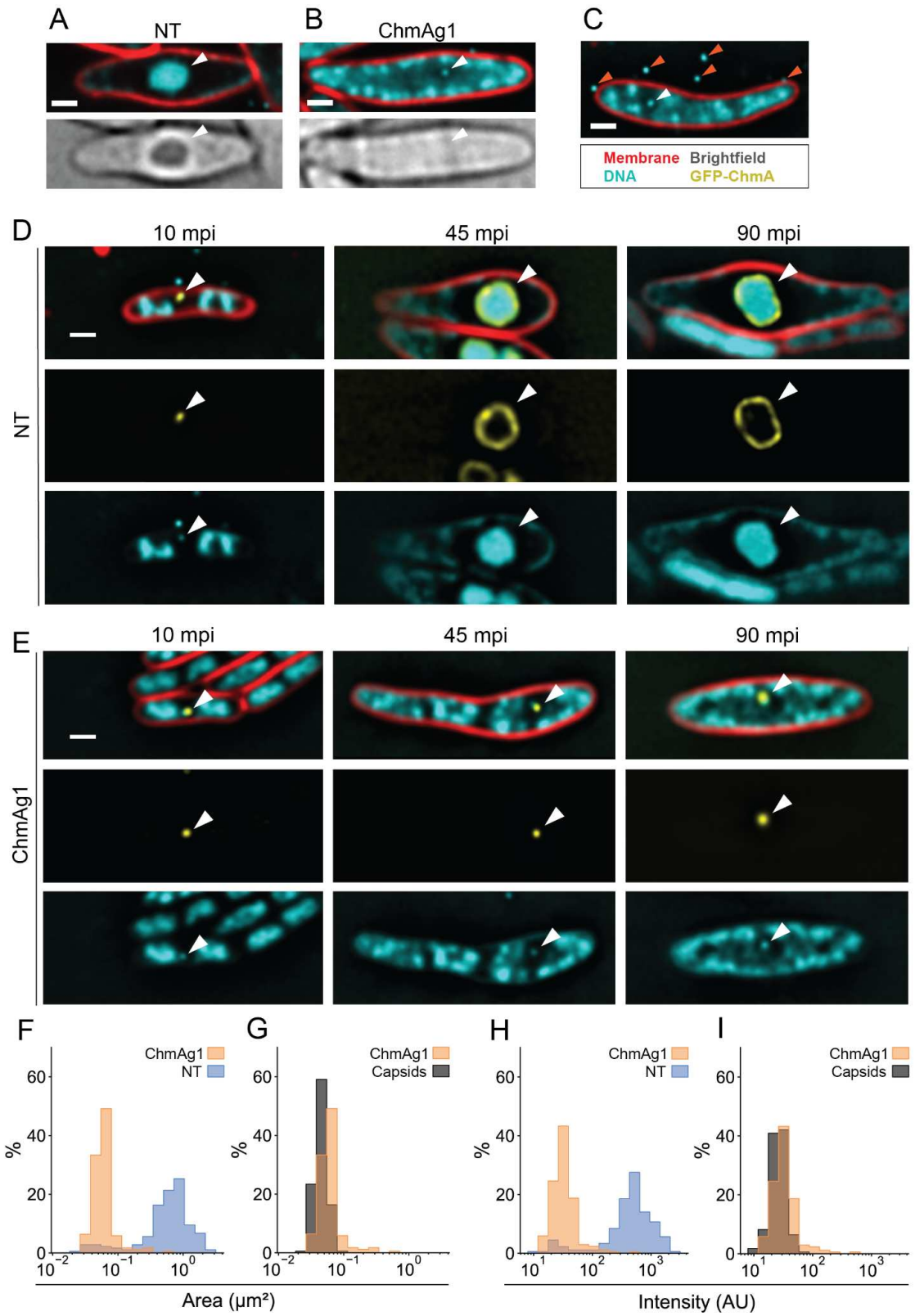

Figure 2 | ChmA knockdown prevents phage genome replication. a, Goslar-infected non-targeting cell 90 mpi. **b**, Goslar-infected knockdown cell 90 mpi. **c**, Goslar-infected knockdown cell with indicated intracellular phage DNA (white arrow) and extracellular phage particles (orange arrows). **d-e**, Time-course of Goslar infection with sfGFP-ChmA in the non-targeting (**d**) and knockdown (**e**) strains. **f-i**, Histograms comparing the cross-sectional area (**f** and **g**) and intensity (**h** and **i**) of DAPI-stained intracellular phage DNA as well as extracellular phage (Capsids, n = 171) during Goslar infection of the non-targeting (NT, n = 178) and knockdown (ChmAg1, n = 171) strains. White arrows indicate phage DNA position as determined by DAPI signal. Scale bars = 1 μm. Cell membranes were stained with FM4-64 (red) and DNA was stained with DAPI (cyan).

We next investigated whether ChmA* complementation restored Goslar DNA replication. Introduction of the empty vector of our second plasmid for ChmA* (FL and ΔCTS) expression did not significantly alter phage nucleus size and DNA quantity in the non-targeting and knockdown strains (**Fig. 3C**). Complementation by untagged, full length, re-

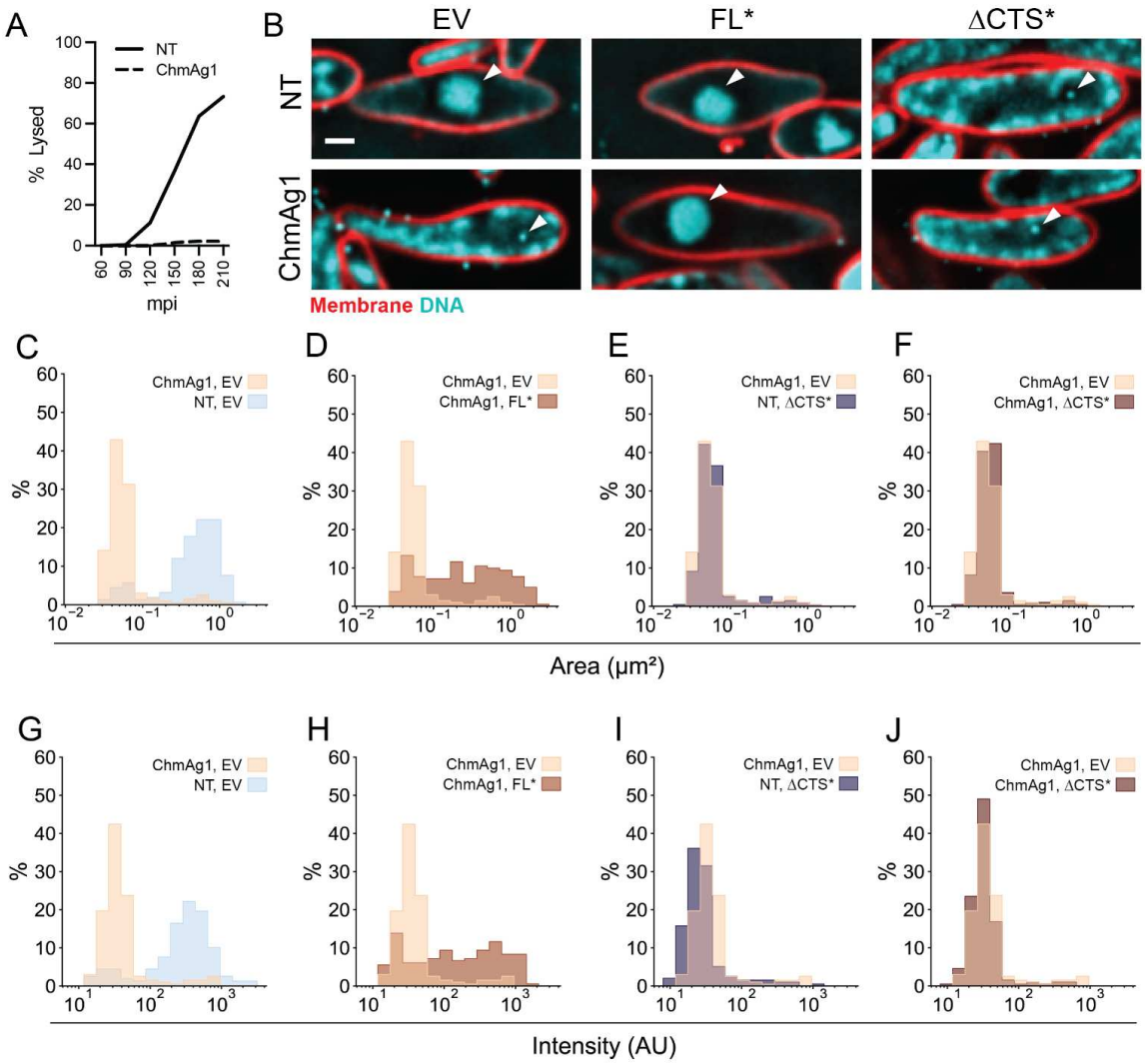

Figure 3 | ChmA* complementation restores phage genome replication. a, Comparison of time-to-lysis for Goslar infections in the non-targeting (NT, n = 248) and knockdown (ChmAg1 = 271) strains. Infected cells were identified by the observation of phage nuclei and/or characteristic cell envelope bulging by brightfield microscopy. **b**, Goslar-infected non-targeting (NT) or knockdown (ChmAg1) cells 90 mpi during expression of full-length (FL*) or truncated (ΔCTS*) ChmA*. EV = empty vector. Cell membranes were stained with FM4-64 (red) and DNA was stained with DAPI (cyan). White arrows indicate phage nuclei. Scale bar = 1 *μ*m. **c-j**, Histograms comparing the cross-sectional area (**c-f**) and intensity (**g-j**) of DAPI-stained intracellular phage DNA during Goslar infection of non-targeting (NT) and knockdown (ChmAg1) strains with or without complementation (EV, FL* or ΔCTS*). Images were collected 90 mpi. n: ChmAg1, EV = 198; NT, EV = 158; ChmAg1, FL* = 181; NT, ΔCTS* = 197; ChmAg1, ΔCTS* = 196.

coded ChmA (FL*, Fig. 1C and G) greatly restored phage nucleus expansion and DNA replication. Although frequently smaller than in the non-targeting strain (**Fig. 3C**), phage DNA area was >0.1 μm² in 70.2% of infections when ChmA-FL* was expressed in the knockdown strain (ChmAg1, FL*; n = 181) compared to 8.6% without ChmA-FL* (ChmAg1, EV; n = 198; **Fig. 3D**). Similarly, phage DNA DAPI intensity was >50 AU, indicating the presence of multiple genome copies (**Fig. 2I**), in 70.2% of infections when ChmA-FL* was expressed in the knockdown strain (ChmAg1, FL*; n = 181) compared to only 14.1% without ChmA-FL* (ChmAg1, EV; n = 198; **Fig. 3H**). In contrast, ChmAΔCTS*, which acts as a dominant negative mutant in plaque assays (**Fig.1F-I**), failed to restore DNA replication during ChmA knockdown and actually inhibited phage nucleus growth and DNA replication in the non-targeting strain (NT, ΔCTS*). When ChmAΔCTS* was expressed, phage DNA area was >0.1 μm2 in 9.1% of non-targeting strain infections (NT, ΔCTS*; n = 197; **Fig. 3E**) and in 5.6% of knockdown strain infections (ChmAg1, ΔCTS*; n = 196; **Fig. 3F**). In keeping with previous results, phage DNA DAPI intensity was also reduced by this dominant negative mutant. ChmAΔCTS* expression resulted in phage DNA DAPI intensity >50 AU in 11.2% of non-targeting strain infections (NT, ΔCTS*; n = 197; **Fig. 3I**) and 7.1% of knockdown strain infections (ChmAg1, ΔCTS*; n = 196; **Fig. 3J**). This independently confirms that ChmA and the phage nucleus compartment are essential for viral genome replication.

A Transcriptionally Active, Membrane-Bound Vesicle Precedes Phage Nucleus Assembly.

The initially injected phage DNA can be visualized as a DAPI-stained punctum in the host cell cytoplasm early in the *Chimalliviridae* life cycle (9, 21). In our fluorescence microscopy studies, Goslar's DNA appeared arrested in a similarly condensed state during ChmA knockdown (**Fig. 2 and 3**). Using cryo-electron tomography (cryo-ET), we have

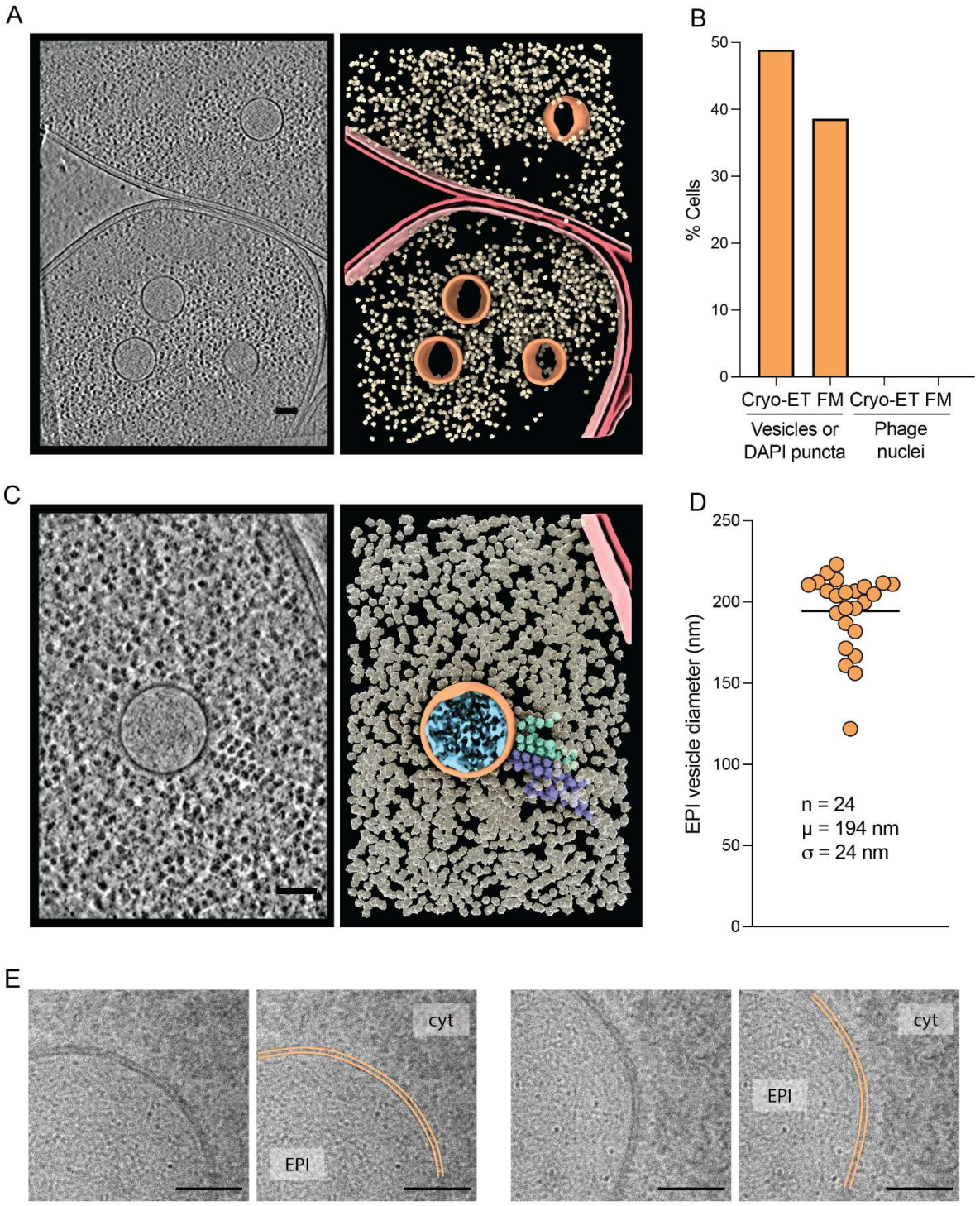

Figure 4 | ChmA knockdown arrests Goslar life cycle at the EPI vesicle stage. a, Slice through a tomogram of knockdown cells 90 mpi containing at least one EPI vesicle (left) and segmentation of the same tomogram (right). **b**, Percentage of cells that contained EPI vesicles by cryo-ET (n = 47) or DAPI-stained puncta by fluorescence microscopy (FM, n = 491) and phage nuclei in the samples examined by cryo-ET. **c**, Slice through a tomogram of an EPI vesicle in the cytoplasm of a knockdown cell 90 mpi with large polysomes extending from the vesicle surface (left) and segmentation of the same tomogram (right). **d**, Plot of the distribution of EPI vesicle diameters. **e**, High-dose 2-D projections of EPI vesicles. The inner and outer leaflets of the lipid bilayer of the EPI vesicle's membrane are traced in orange. Cyt = cytoplasm and EPI = EPI vesicle. In the tomogram segmentations (**a** and **c**), outer and inner membranes are burgundy and pink respectively, ribosomes are yellow, polysomes are light green and purple, EPI vesicle membranes are orange, and DNA within the EPI vesicle is cyan. Scale bars: A and C = 100 nm, E = 50 nm.

recently observed vesicles containing DNA in the cytoplasm of *E. coli* and *P. chlororaphis* cells infected by *Chimalliviridae* phages Goslar and 201phi2-1 respectively (10). Notably, the composition of the interior of these vesicles was the same as the phage nucleus, but using subtomogram analysis we determined that they were surrounded by a lipid bilayer instead of a ChmA coat. We called these vesicles unidentified spherical bodies (USBs) and speculated that they may represent a pre-nuclear stage in the phage life

cycle, providing protection for the initially injected viral genome before assembly of the phage nucleus (10).

Based on these observations, we hypothesized that in the absence of ChmA, the injected Goslar genome was trapped within this vesicle. Using cryo-ET, we observed that at 90 mpi, 48.9% of knockdown cells (n = 47, **Fig. 4B**) contained vesicles with an average diameter of 194 ± 24 nm, similar to previously observed USBs enclosed by a lipid bilayer (n = 24, **Fig. 4A, D and E**). The lipid bilayer nature of these vesicles, which were similar in size to the previously observed USBs (10), was evident from direct visualization in the tomograms showing two leaflets of high density corresponding to the head groups, and an intermediate region of low density corresponding to the lipid tails, with an overall thickness of ~4 nm (**Fig. 4E and Fig. S5**). No cells had a ChmA phage nucleus, consistent with the lack of phage nuclei observed in cells from the same sample via fluorescence microscopy (**Fig. 4B**). Additionally, DAPI-stained puncta of phage DNA were detected in cells from the same sample at a comparable frequency as the vesicles were observed by cryo-ET (38.6%, n = 491; **Fig. 4B**). Thus, before assembly of the ChmA phage nucleus, the injected *Chimalliviridae* genome is initially enclosed in a lipid bilayer, a structure we name the early phage infection (EPI) vesicle.

It was previously unclear whether the EPI vesicles represented a stage of the viral life cycle or were failed or aborted infections (10). Surprisingly, we observed polysomes containing at least 10 ribosomes extending from the surface of EPI vesicles (**Fig. 4C**), demonstrating that these structures are highly transcriptionally active. *Chimalliviridae* phages use two multisubunit RNA polymerases to carry out transcription: a virion RNA polymerase (vRNAP) and non-virion RNA polymerase (nvRNAP). The vRNAP is packaged into the capsids and injected into the host cell with the viral DNA to transcribe early phage genes (22–24). Based on the organization of polysomes extending from the EPI vesicle surface, it is likely that the vRNAP is injected with the genome into the EPI vesicle, where it transcribes mRNAs that are exported to the cytoplasm and translated. Indeed, Antonova et al. recently showed that vRNAP subunit gp180 of *Chimallviridae* phage PhiKZ colocalizes with the initially injected phage DNA via fluorescence microscopy (25). We used mass spectrometry to determine whether initial phage gene expression occurs in the absence of ChmA. During ChmA knockdown, many viral proteins were detected at 30 mpi (**Fig. 5A, Table S1**). Among the most abundant viral proteins detected, statistically significant reduction in expression was only observed for ChmA itself, further demonstrating that the EPI vesicle is transcriptionally active and is a bona fide stage in the *Chimalliviridae* life cycle.

The ChmA-enclosed phage nucleus selectively imports both host and phage proteins, concentrating DNA replication machinery within this compartment (6, 7, 26, 27). We hypothesized that the membrane-enclosed EPI vesicle lacks this import ability, thereby preventing accumulation of these key enzymes. To test this idea, we investigated the

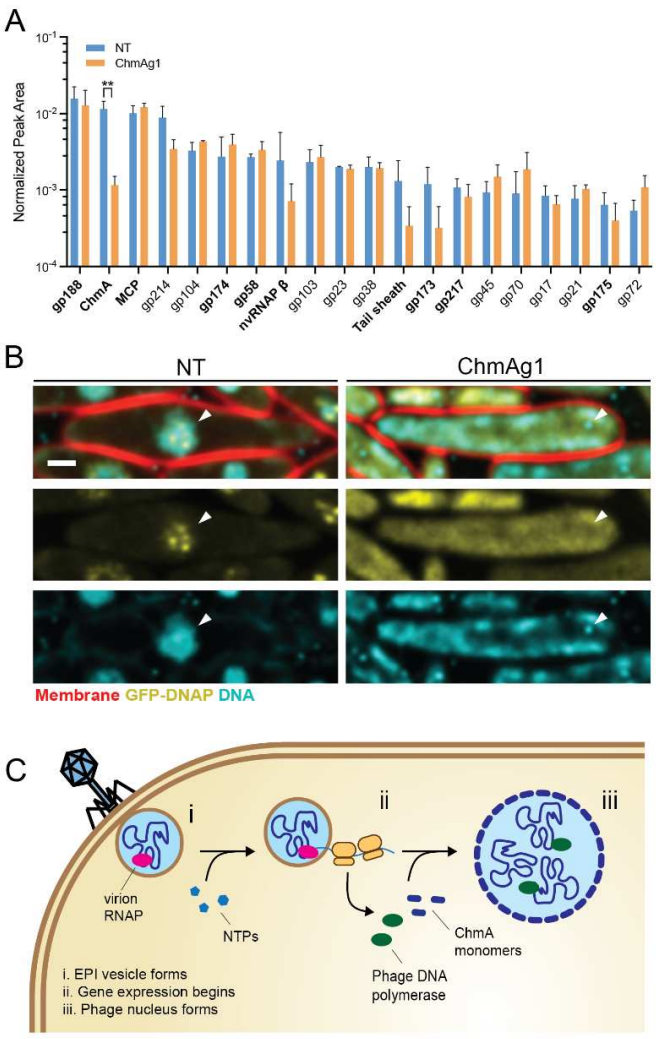

Figure 5 I ChmA knockdown effects on major processes of early infection. a, Average peak area of the 20 most abundant Goslar proteins detected by label free quantification mass spectrometry of Goslar-infected cells 30 mpi. Proteins encoded by genes in the *Chimalliviridae* core genome (8) are in bold. ** $p < 0.01$. **b**, Localization of GFP-tagged Goslar DNA polymerase (sfGFP-DNAPGos) in non-targeting (NT) and knockdown (ChmAg1) cells 90 mpi. Cell membranes were stained with FM4-64 (red) and DNA was stained with DAPI (cyan). White arrows indicate phage DNA position determined by DAPI signal. Scale bar = 1 μm. **c**, Schematic of early *Chimalliviridae* infection. i) Goslar injects its genome along with its virion RNA polymerase (vRNAP, pink) into the membrane-bound EPI vesicle. ii) Supported by nucleotide import into the EPI vesicle (light blue), early viral genes are transcribed by the vRNAP and the mRNAs are exported to the cytoplasm for translation by host ribosomes (yellow). iii) The viral genome is transferred from the EPI vesicle to the ChmA phage nucleus (dark blue). At this stage, the viral DNA polymerase (green) can be imported into the phage nucleus and DNA replication begins.

localization of GFP-tagged Goslar DNA polymerase gp244 (sfGFP-DNAP$_{Gos}$) during ChmA knockdown. sfGFP-DNAP$_{Gos}$ localized within the phage nucleus in our control strain, forming foci on the phage DNA. However, when ChmA was knocked down, sfGFP-DNAP$_{Gos}$ remained diffuse throughout the host cell cytoplasm and failed to colocalize with the EPI vesicle (**Fig. 5B**). This suggests that the DNA replication machinery cannot access the injected phage genome in the EPI vesicles, potentially explaining why ChmA knockdown inhibits phage DNA replication while early phage gene expression, which is driven by the injected vRNAP, is unaffected.

Discussion

In this study, we demonstrated that the phage nucleus is required for nucleus-forming phage DNA replication. Similar to replication compartments of eukaryotic viruses, which are believed to have evolved in response to host defenses, the phage nucleus may have originated as a protective mechanism against bacterial immune systems but is now intrinsically essential for the phage life cycle. We also demonstrated that infection is initiated through formation of a membrane-bound vesicle containing the injected genome, which we name the early phage infection (EPI) vesicle (**Fig. 5C**). EPI vesicles, which we hypothesize are formed from the host inner membrane during injection, are transcriptionally active and therefore must have yet-to-be identified mechanisms for importing nucleotides from and exporting mRNA to the cytoplasm. These early infection functions are likely mediated by *Chimalliviridae* proteins such as the vRNA polymerase that are packaged into phage capsids and injected into host cells (22, 23, 28, 29). After the early phage gene expression program is initiated, the phage genome becomes enclosed within the proteinaceous phage nucleus to carry out genome replication and proceed through the rest of its life cycle. Using membranes to decouple transcription from translation is a hallmark of eukaryotic cells but has never been observed before in prokaryotes. The discovery of this early membrane-bound intermediate also resolves the question of how *Chimalliviridae* protect their genomes from host DNA-targeting defense systems before the proteinaceous nuclear shell is synthesized. Thus, *Chimalliviridae* form sophisticated subcellular compartments of distinct compositions and functions that facilitate successive stages of the life cycle.

References

1. D. M. Knipe, A. Prichard, S. Sharma, J. Pogliano, Replication compartments of eukaryotic and bacterial DNA viruses: Common themes between different domains of host cells. Annu. Rev. Virol. 9, 307–327 (2022).
2. Q. Nevers, A. A. Albertini, C. Lagaudrière-Gesbert, Y. Gaudin, Negri bodies and other virus membrane-less replication compartments. Biochim. Biophys. Acta Mol. Cell Res. 1867, 118831 (2020).
3. M. Schmid, T. Speiseder, T. Dobner, R. A. Gonzalez, DNA virus replication compartments. J. Virol. 88, 1404–1420 (2014).
4. V. Chaikeeratisak, E. A. Birkholz, J. Pogliano, The Phage Nucleus and PhuZ Spindle: Defining Features of the Subcellular Organization and Speciation of Nucleus-Forming Jumbo Phages. Front. Microbiol. 12, 641317 (2021).
5. L. M. Malone, S. L. Warring, S. A. Jackson, C. Warnecke, P. P. Gardner, L. F. Gumy, P. C. Fineran, A jumbo phage that forms a nucleus-like structure evades CRISPR–Cas DNA targeting but is vulnerable to type III RNA-based immunity. Nature Microbiology. 5, 48–55 (2019).
6. S. D. Mendoza, E. S. Nieweglowska, S. Govindarajan, L. M. Leon, J. D. Berry, A. Tiwari, V. Chaikeeratisak, J. Pogliano, D. A. Agard, J. Bondy-Denomy, A bacteriophage nucleus-like compartment shields DNA from CRISPR nucleases. Nature. 577, 244–248 (2020).
7. V. Chaikeeratisak, K. Nguyen, K. Khanna, A. F. Brilot, M. L. Erb, J. K. C. Coker, A. Vavilina, G. L. Newton, R. Buschauer, K. Pogliano, E. Villa, D. A. Agard, J. Pogliano, Assembly of a nucleus-like structure during viral replication in bacteria. Science. 355, 194–197 (2017).
8. A. Prichard, J. Lee, T. G. Laughlin, A. Lee, K. P. Thomas, A. E. Sy, T. Spencer, A. Asavavimol, A. Cafferata, M. Cameron, N. Chiu, D. Davydov, I. Desai, G. Diaz, M. Guereca, K. Hearst, L. Huang, E. Jacobs, A. Johnson, S. Kahn, R. Koch, A. Martinez, M. Norquist, T. Pau, G. Prasad, K. Saam, M. Sandhu, A. J. Sarabia, S. Schumaker, A. Sonin, A. Uyeno, A. Zhao, K. D. Corbett, K. Pogliano, J. Meyer, J. H. Grose, E. Villa, R. Dutton, J. Pogliano, Identifying the core genome of the nucleus-forming bacteriophage family and characterization of Erwinia phage RAY. Cell Rep. 42, 112432 (2023).
9. E. A. Birkholz, T. G. Laughlin, E. Armbruster, S. Suslov, J. Lee, J. Wittmann, K. D. Corbett, E. Villa, J. Pogliano, A cytoskeletal vortex drives phage nucleus rotation during jumbo phage replication in E. coli. Cell Rep. 40, 111179 (2022).
10. T. G. Laughlin, A. Deep, A. M. Prichard, C. Seitz, Y. Gu, E. Enustun, S. Suslov, K. Khanna, E. A. Birkholz, E. Armbruster, J. A. McCammon, R. E. Amaro, J. Pogliano, K. D. Corbett, E. Villa, Architecture and self-assembly of the jumbo bacteriophage nuclear shell. Nature. 608, 429–435 (2022).
11. E. S. Nieweglowska, A. F. Brilot, M. Méndez-Moran, C. Kokontis, M. Baek, J. Li, Y. Cheng, D. Baker, J. Bondy-Denomy, D. A. Agard, The φPA3 phage nucleus is enclosed by a self-assembling 2D crystalline lattice. Nat. Commun. 14, 927 (2023).
12. B. A. Adler, M. J. Al-Shimary, J. R. Patel, E. Armbruster, E. Charles, K. Miller, A. Lahiri, M. Trinidad, S. Beurnier, A. L. Azadeh, R. Barrangou, V. K. Mutalik, J. S. Schoeniger, J. A. Pogliano, D. F. Savage, J. A. Doudna, B. F. Cress, Targeted RNA Knockdown Unveils the Functional Genomes of Bacteriophages. In Preparation.
13. E. J. Charles, S. E. Kim, G. J. Knott, D. Smock, J. Doudna, D. F. Savage, Engineering improved Cas13 effectors for targeted post-transcriptional regulation of gene expression. bioRxiv (2021), p. 2021.05.26.445687.
14. M. R. O'Connell, Molecular Mechanisms of RNA Targeting by Cas13-containing Type VI CRISPR–Cas Systems. J. Mol. Biol. 431, 66–87 (2019).
15. I. Jain, M. Kolesnik, L. Minakhin, N. Morozova, A. Shiriaeva, A. Kirillov, S. Medvedeva, K. Kuznedelov, S. Borukhov, K. S. Makarova, E. V. Koonin, K. Severinov, E. Semenova, tRNA anticodon cleavage by target-activated CRISPR-Cas13a effector. bioRxiv (2021), p. 2021.11.10.468108.
16. A. East-Seletsky, M. R. O'Connell, S. C. Knight, D. Burstein, J. H. D. Cate, R. Tjian, J. A. Doudna, Two distinct RNase activities of CRISPR-C2c2 enable guide-RNA processing and RNA detection. Nature. 538, 270–273 (2016).
17. B. A. Adler, T. Hessler, B. F. Cress, A. Lahiri, V. K. Mutalik, R. Barrangou, J. Banfield, J. A. Doudna, Broad-spectrum CRISPR-Cas13a enables efficient phage genome editing. Nat Microbiol. 7, 1967–1979 (2022).
18. O. O. Abudayyeh, J. S. Gootenberg, S. Konermann, J. Joung, I. M. Slaymaker, D. B. T. Cox, S. Shmakov, K. S. Makarova, E. Semenova, L. Minakhin, K. Severinov, A. Regev, E. S. Lander, E. V. Koonin, F. Zhang, C2c2 is a single-component programmable RNA-guided RNA-targeting CRISPR effector. Science. 353, aaf5573 (2016).
19. P. B. Otoupal, B. F. Cress, J. A. Doudna, J. S. Schoeniger, CRISPR-RNAa: targeted activation of translation using dCas13 fusions to translation initiation factors. Nucleic Acids Res. 50, 8986–8998 (2022).
20. V. Chaikeeratisak, E. A. Birkholz, A. M. Prichard, M. E. Egan, A. Mylvara, P. Nonejuie, K. T. Nguyen, J. Sugie, J. R. Meyer, J. Pogliano, Viral speciation through subcellular genetic isolation and virogenesis incompatibility. Nat. Commun. 12, 1–9 (2021).
21. V. Chaikeeratisak, K. Khanna, K. T. Nguyen, M. E. Egan, E. Enustun, E. Armbruster, J. Lee, K. Pogliano, E. Villa, J. Pogliano, Subcellular organization of viral particles during maturation of nucleus-forming jumbo phage. Sci Adv. 8, eabj9670 (2022).
22. P.-J. Ceyssens, L. Minakhin, A. Van den Bossche, M. Yakunina, E. Klimuk, B. Blasdel, J. De Smet, J.-P. Noben, U. Bläsi, K. Severinov, R. Lavigne, Development of giant bacteriophage ϕKZ is independent of the host transcription apparatus. J. Virol. 88, 10501–10510 (2014).
23. J. A. Thomas, M. R. Rolando, C. A. Carroll, P. S. Shen, D. M. Belnap, S. T. Weintraub, P. Serwer, S. C. Hardies, Characterization of Pseudomonas chlororaphis myovirus 201ϕ2-1 via genomic sequencing, mass spectrometry, and electron microscopy. Virology. 376, 330–338 (2008).
24. M. Yakunina, T. Artamonova, S. Borukhov, K. S. Makarova, K. Severinov, L. Minakhin, A non-canonical multisubunit RNA polymerase encoded by a giant bacteriophage. Nucleic Acids Res. 43, 10411–10420 (2015).
25. D. Antonova, V. V. Belousova, E. Zhivkoplyas, M. Sobinina, T. Artamonova, I. E. Vishnyakov, I. Kurdyumova, A. Arseniev, N. Morozova, K. Severinov, M. Khodorkovskii, M. V. Yakunina, The Dynamics of Synthesis and Localization of Jumbo Phage RNA Polymerases inside Infected Cells. bioRxiv (2023), p. 2023.09.14.557509.
26. K. T. Nguyen, J. Sugie, K. Khanna, M. E. Egan, E. A. Birkholz, J. Lee, C. Beierschmitt, E. Villa, J. Pogliano, Selective transport of fluorescent proteins into the phage nucleus. PLoS One. 16, e0251429 (2021).

27. E. Lecoutere, P.-J. Ceyssens, K. A. Miroshnikov, V. V. Mesyanzhinov, V. N. Krylov, J.-P. Noben, J. Robben, K. Hertveldt, G. Volckaert, R. Lavigne, Identification and comparative analysis of the structural proteomes of phiKZ and EL, two giant Pseudomonas aeruginosa bacteriophages. Proteomics. 9, 3215–3219 (2009).
28. J. A. Thomas, S. T. Weintraub, W. Wu, D. C. Winkler, N. Cheng, A. C. Steven, L. W. Black, Extensive proteolysis of head and inner body proteins by a morphogenetic protease in the giant Pseudomonas aeruginosa phage φKZ. Mol. Microbiol. 84, 324–339 (2012).
29. V. N. Krylov, T. A. Smirnova, I. B. Minenkova, T. G. Plotnikova, I. Z. Zhazikov, E. A. Khrenova, Pseudomonas bacteriophage phi KZ contains an inner body in its capsid. Can. J. Microbiol. 30, 758–762 (1984).
30. M. J. Casadaban, S. N. Cohen, Analysis of gene control signals by DNA fusion and cloning in Escherichia coli. J. Mol. Biol. 138, 179–207 (1980).
31. V. Lam, E. Villa, Practical Approaches for Cryo-FIB Milling and Applications for Cellular Cryo-Electron Tomography. Methods Mol. Biol. 2215, 49–82 (2021).
32. D. N. Mastronarde, Automated electron microscope tomography using robust prediction of specimen movements. J. Struct. Biol. 152, 36–51 (2005).
33. F. Eisenstein, H. Yanagisawa, H. Kashihara, M. Kikkawa, S. Tsukita, R. Danev, Parallel cryo electron tomography on in situ lamellae. Nat. Methods. 20, 131–138 (2023).
34. D. Tegunov, P. Cramer, Real-time cryo-electron microscopy data preprocessing with Warp. Nat. Methods. 16, 1146–1152 (2019).
35. S. Zheng, G. Wolff, G. Greenan, Z. Chen, F. G. A. Faas, M. Bárcena, A. J. Koster, Y. Cheng, D. A. Agard, AreTomo: An integrated software package for automated marker-free, motion-corrected cryo-electron tomographic alignment and reconstruction. J Struct Biol X. 6, 100068 (2022).
36. L. Lamm, R. D. Righetto, W. Wietrzynski, M. Pöge, A. Martinez-Sanchez, T. Peng, B. D. Engel, MemBrain: A deep learning-aided pipeline for detection of membrane proteins in Cryo-electron tomograms. Comput. Methods Programs Biomed. 224, 106990 (2022).
37. D. N. Mastronarde, S. R. Held, Automated tilt series alignment and tomographic reconstruction in IMOD. J. Struct. Biol. 197, 102–113 (2017).
38. C. F. Jekel, G. Venter, M. P. Venter, Obtaining a hyperelastic non-linear orthotropic material model via inverse bubble inflation analysis. Struct. Multidiscip. Optim. 54, 927–935 (2016).
39. T. Wagner, F. Merino, M. Stabrin, T. Moriya, C. Antoni, A. Apelbaum, P. Hagel, O. Sitsel, T. Raisch, D. Prumbaum, D. Quentin, D. Roderer, S. Tacke, B. Siebolds, E. Schubert, T. R. Shaikh, P. Lill, C. Gatsogiannis, S. Raunser, SPHIRE-crYOLO is a fast and accurate fully automated particle picker for cryo-EM. Commun Biol. 2, 218 (2019).
40. J. Zivanov, T. Nakane, B. O. Forsberg, D. Kimanius, W. J. Hagen, E. Lindahl, S. H. Scheres, New tools for automated high-resolution cryo-EM structure determination in RELION-3. Elife. 7 (2018), doi:10.7554/eLife.42166.
41. A. Hagberg, P. J. Swart, D. A. Schult, "Exploring network structure, dynamics, and function using NetworkX" (LA-UR-08–05495; LA-UR-08–5495, Los Alamos National Laboratory (LANL), Los Alamos, NM (United States), 2008), (available at https://www.osti.gov/biblio/960616).
42. E. F. Pettersen, T. D. Goddard, C. C. Huang, E. C. Meng, G. S. Couch, T. I. Croll, J. H. Morris, T. E. Ferrin, UCSF ChimeraX: Structure visualization for researchers, educators, and developers. Protein Sci. 30, 70–82 (2021).
43. U. H. Ermel, S. M. Arghittu, A. S. Frangakis, ArtiaX: An electron tomography toolbox for the interactive handling of sub-tomograms in UCSF ChimeraX. Protein Sci. 31, e4472 (2022).

Acknowledgements

We thank the members of the Emerging Pathogens Initiative HHMI Consortium for their feedback and support. J.H. is an EMBO long-term postdoctoral Fellow. Z.K.R. is supported and E.G.A. was previously supported by an NIH PiBS training grant (T32 grant GM133351). J.A.D., D.F.S. and E.V. are investigators of the Howard Hughes Medical Institute. We acknowledge the use of the UC San Diego cryo-EM facility, which was built and equipped with funds from UC San Diego and an initial gift from the Agouron Institute. The authors acknowledge funding from the Howard Hughes Medical Institute through the Emerging Pathogens Initiative grant (to E.V., J.P., K.D.C., and K.P.), the National Institutes of Health grants R01-GM129245 (to J.P. and E.V.), R35 GM144121 (to K.D.C.), MRI grant NSF DBI 1920374 (to E.V.) and R01-GM57045 (to K.P.), InCoGenTEC (to B.F.C. and J.A.D.), m-CAFEs (B.A.A. and J.A.D.), and the Curci Foundation (B.F.C.). This paper was typeset with a bioRxiv template by @Chrelli: www.github.com/chrelli/bioRxiv-word-template

Author contributions

Conceptualization: E.G.A., K.P., E.V., J.P.; Methodology: E.G.A., J.L., B.A.A., E.C., B.F.C., D.F.S., J.A.D., J.H.; Investigation: E.G.A., J.L., A.R.V., E.E., A.A., A.D., Z.K.R., C.J.M., M.G., J.P.; Visualization: E.G.A., J.L., J.H., E.E., B.A.A.; Project administration: E.G.A., J.P., E.V.; Supervision: E.V., J.P., K.P.; Writing – original draft: E.G.A., J.P., E.V., K.D.C.; Writing – review & editing: All authors contributed to reviewing and editing this manuscript.

Competing interest statement

K.P. and J.P. have an equity interest in Linnaeus Bioscience Incorporated and receive income. The terms of this arrangement have been reviewed and approved by the University of California, San Diego, in accordance with its conflict-of-interest policies. The Regents of the University of California have patents issued and pending for CRISPR technologies on which J.A.D., B.F.C., B.A.A., D.F.S., E.C., J.P., K.P., E.G.A. and J.L. are inventors. J.A.D. is a cofounder of Caribou Biosciences, Editas Medicine, Scribe Therapeutics, Intellia Therapeutics, and Mammoth Biosciences. J.A.D. is a scientific advisory board member of Vertex, Caribou Biosciences, Intellia Therapeutics, Scribe Therapeutics, Mammoth Biosciences, Algen Biotechnologies, Felix Biosciences, The Column Group, and Inari. J.A.D. is Chief Science Advisor to Sixth Street, a Director at Johnson & Johnson, Altos and Tempus, and has research projects sponsored by Apple Tree Partners and Roche. D.F.S. is a cofounder and scientific advisory board member of Scribe Therapeutics.

Data availability

The mass spectrometry proteomics data have been deposited to the ProteomeXchange Consortium via the PRIDE partner repository with the dataset identifier PXD045200 and 10.6019/PXD045200. Any additional information required to reanalyze the data reported in this paper is available from the corresponding authors upon request.

Materials and Methods

Bacterial growth conditions.

Table S2 lists the bacterial strains used in this study. All strains were generated from lab strain Escherichia coli MC1000, which was originally derived from MG1655 (30). Strains were grown on Luria-Bertani (LB) plates containing 10 g Bacto-Tryptone, 5 g NaCl, 5 g Bacto-yeast extract and 16 g agar per liter ddH2O with appropriate antibiotics to maintain plasmids. Liquid cultures were generated by inoculating LB with single colonies. p15A-CmR backbone plasmids (see table S2) were maintained using 30 µg/mL chloramphenicol (Sigma-Aldrich) in plates, imaging pads and liquid cultures. dRfxCas13d expression was induced by aTc (anhydrotetracycline, Cayman Chemical Company) as indicated. pDW206 plasmids (see table S2) were similarly maintained using 100 µg/mL ampicillin (Cayman Chemical Company) and protein expression was induced by IPTG (isopropyl ß-D-1-thiogalactopyranoside, Teknova) as indicated. See additional details on induction conditions in specific procedure methods below. Streak plates were incubated overnight at 37°C.

Bacteriophage preparation.

We originally acquired phage Goslar from Johannes Wittman at the DSMZ (*9*). Goslar lysates were amplified as follows. 10 uL of high titer lysate, 500 uL of *E. coli* MC1000 overnight liquid culture and 4.5 mL of LB top agar (0.35%) were mixed and plated on 3-5 LB plates, then incubated overnight at 37 °C. The next day, 5 mL of chilled LB broth were added to each plate and incubated ~5 hours at room temperature. All liquid was then drawn off of the plates into a single tube and centrifuged at 3220 x g for 10 minutes. The supernatant was transferred to a new tube and cleared with chloroform (3 drops chloroform/5 mL lysate). After 10 minutes incubating at room temperature with periodic mixing by inversion, the aqueous phase of the lysate was filtered through a 0.45 µm Corning membrane filter by syringe into a sterile conical tube and stored at 4°C.

Plasmid construction, spacer design and bacterial transformation.

Plasmids and crRNA spacer sequences used are listed in table S2 and S3. dRfxCas13d and guides were co-expressed from a p15A-CmR vector, while sfGFP, sfGFP fusions, ChmA* and ChmA*ΔCTS were expressed from vector pDSW206 (9). The initial p15A-CmR backbone dRfxCas13d entry vector and non-targeting guide plasmids were generously provided by the

Doudna and Savage labs (13). All other plasmids were designed manually in Benchling, then synthesized by GenScript and delivered lyophilized.

We manually designed the two chmA transcript targeting crRNA spacers to be 31 bp long and reverse complementary to the 5' end of the Goslar chmA ORF, following the same design conventions described in Adler et al. (12) (**Fig. 1C**). Goslar's chmA ORF ends 92 bp upstream of the following non-virion RNA polymerase subunit (nvRNAP β' 1) gene, which has its own RBS (aggaga) 6 bp upstream of its ATG site, strongly indicating that these genes are translated independently. Our non-targeting control was a previously validated crRNA targeting the T4 phage major capsid protein (17).

GenScript plasmids were hydrated at 200 µg/mL and diluted to 20 µg/mL in dH2O. 1 µL diluted plasmid was added to 30-50 µL of electroporation competent *E. coli*, which were prepared by washing in 10% glycerol, and electroporated with 2.5 kV. After transformants recovered in 1 mL SOC at 37°C for 60 minutes, they were spread on LB plates with appropriate antibiotics and incubated overnight at 37°C.

Western blot.

For 200 µL of OD_{600} 0.2 cells were spread on 1% agarose, 25% LB, 6 cm diameter plates containing 30 ug/mL chloramphenicol and 5 nM aTc. After incubating at 37°C for 2 hours inside a humidor, cells were infected with 100 µL ~10^{10} PFU/mL Goslar lysate and incubated again at 37°C. 90 mpi, cells were collected by the addition of 1 mL of 25% LB to each pad and gentle scraping with the bottom of an Eppendorf tube followed by aspiration. After checking the OD_{600} via nanodrop, ~4.0 x 10^8 cells were spun down for 1 minute at 211 x g and resuspended in 100 µL 2x SDS loading buffer (0.1 M Tris HCl, 0.004% bromophenol blue, 4% SDS, 20% glycerol, pH 6.8 plus 5% BME). Samples were boiled for 4 minutes at 95°C and vortexed for 30 seconds. After being diluted 1:5 in the same loading buffer, 10 µL of each sample were loaded into a Novex 4-20% Tris-Glycine Gel and run at 150 V. Protein was transferred to PVDF (Pall Life Sciences) and blocked by incubation at room temperature with StartingBlock Blocking Buffer (Thermo Scientific). The membrane was cut below the 130 kDa molecular weight marker band to separate the regions containing ChmA and RpoB (loading control). The membrane sections were then incubated overnight at 4°C with the corresponding antibody: anti-ChmA (dilution = 1:500; custom GenScript polyclonal rabbit antibody), HRP-conjugated mouse anti-RpoB (dilution = 1:5,000; Biolegend Cat# 663907, RRID:AB_2629625). RpoB is the *E. coli* RNA polymerase β subunit. The membranes were washed three times for 15 minutes with TBS-T and the ChmA-containing membrane was incubated with HRP-conjugated goat anti-rabbit IgG (H + L) secondary antibody (dilution = 1:10,000; Thermo Fisher Scientific Cat# 65-6120, RRID:AB_2533967) for 1.5 hrs at room temperature and washed as before with TBS-T. The membranes were treated with ECL western blotting detection reagent (Cytiva Amersham) and imaged using a ChemiDoc MP Imaging System (Bio-Rad). The amido black imaging setting was used to image the molecular weight marker ladder and chemiluminescence setting for visualizing the target protein bands. Figure panels were generated in Adobe Photoshop (21.2.0) and Adobe Illustrator (24.2). The western blot in **Fig. 1C** was run in biological and technical triplicate.

Antibody generation.

For the expression and purification of Goslar ChmA protein, the gene was cloned into UC Berkeley Macrolab vectors 2-BT (addgene #29666) for N-terminal TEV protease-cleavable His6-tag constructs. For protein expression, the construct was transformed into *E. coli* Rosetta2 pLysS (EMD Millipore), and the transformants were obtained on the nutrient agar plates containing carbenicillin and chloramphenicol antibiotics. A single transformant colony was inoculated into LB medium, and the culture was allowed to grow overnight in a 37°C incubator shaker. The following morning, the overnight culture (5 mL) was used to inoculate 1 L 2XYT medium and allowed to grow until the growth reached an OD_{600} of 0.6-0.8. This was followed by induction with 0.33 mM IPTG. The induced cultures were incubated overnight at 20°C for the further expression of ChmA protein. Subsequently, the cells were harvested by centrifugation, and the bacterial pellets were resuspended in ice-cold resuspension buffer containing 50 mM Tris, pH 7.5, 300 mM NaCl, 10 mM imidazole, 10% glycerol, and 2 mM β-mercaptoethanol. Resuspended cells were subjected to lysis using a sonicator, and the lysate was clarified using centrifugation. The protein was purified using Ni2+ affinity chromatography. Eluted protein was concentrated, and buffer exchanged to remove imidazole, and the N-terminal His6-tag was cleaved using TEV protease. The tag-cleaved protein was further subjected to purification by size exclusion chromatography using a Superdex 200 Increase 10/300 GL column (Cytiva) in a buffer containing 20 mM Tris, pH 7.4, 250 mM NaCl, and 2 mM β-mercaptoethanol. Finally, the quality of purified protein was assessed by running an SDS-PAGE, and the protein aliquots (~2 mg/mL concentration) were flash-frozen using liquid nitrogen and stored at -80°C until shipment for antibody generation. GenScript generated polyclonal αChmA rabbit antibodies via their Polyexpress method, which were stored at -20°C upon being received.

Plaque Assay.

All plaque assays were performed in biological triplicate. 1 mL of overnight culture (no preinduction) was mixed with 9 mL of 0.35% LB top agar containing antibiotics and inducing agents and poured onto 25 mL LB plates containing the required antibiotics. As the plates did not contain inducing agents, aTc and IPTG were added to the top agar at initial concentrations to account for diffusion into the total final plate volume. For all plaque assays involving dRfxCas13d-expressing strains (**Fig. 1E-F, H-I**), aTc = 5 nM. For all plaque assays involving ChmA*- or ChmA*ΔCTS-expressing strains (**Fig. 1H-I and Fig. S2**), IPTG = 2 mM. Plates were spotted with a 10-fold dilution series of Goslar from 10^1-10^8 (prepared in LB) in technical triplicate with 3 µL/spot and were dried in a biosafety cabinet with lids removed. Once the spots dried (6-10 minutes), the plates were incubated at 37°C for 15-18 hours. Plates were photographed using an iPhone 13 camera and efficiency of plaquing was recorded. Viral reproduction inhibition via ChmA knockdown or ChmA*ΔCTS expression frequently precluded countable plaque formation and instead produced faint zones of clearing at higher dilutions. In these cases, the most concentrated dilution at which no clearing was observed was treated as 1 PFU. Figure panels were generated using Adobe Photoshop (21.2.0) and Adobe Illustrator (24.2). Data analysis was performed in Microsoft Excel (version 16.75.2) and GraphPad Prism (version 10.0.0 (131)) and graphs were generated in Graphpad Prism.

Live single cell static fluorescence microscopy and time-lapse microscopy.

Fluorescence microscopy and time-lapse microscopy experiments were performed in at least biological duplicate. Host cells were suspended in 25% LB at OD_{600} 0.4 as measured by nanodrop. 5 uL were spotted and spread on the surface of 1% agarose, 25% LB imaging pads containing required antibiotics and inducing agents on single-well concavity glass slides, then incubated for 1.5 to 2 hours at 37°C without coverslips in a humidor. 10 µL of ~10^{10} PFU/mL Goslar lysate were spotted and spread onto the imaging pads and the pads were incubated further at 37°C until the desired infection time point. For all microscopy experiments, aTc in imaging pads = 5 nM. Plasmid leakiness in the absence of IPTG was sufficient to express sfGFP-ChmA and sfGFP at appropriately low levels for related experiments (**Fig. 2D-E and Fig. S4**). To induce ChmA* and ChmAΔCTS* expression (**Fig. 3B-J**), 8 uL of 2 mM IPTG was spread on the pad surface 20 minutes before Goslar infection.

All live cell microscopy was performed on a DeltaVision Elite Deconvolution microscope (Applied Precision, Issaquah, WA, USA). Directly before imaging, a glass coverslip was placed on top of the agarose pad. For static fluorescence microscopy, imaging pads were stained with 8 µL of dye mix (25 µg/mL DAPI, 3.75 µg/mL FM4-64) at room temperature 5 minutes before imaging. DAPI: Thermo Fisher Scientific Cat# D1306, FM4-64: Thermo Fisher Scientific Cat# T13320. Cells were imaged with 8-20 slices in the Z-axis at 0.2 µm increments. For time-lapses, no fluorescent stains were used and cells were imaged in 12 or 20 slices in the Z-axis at 5 minute intervals with Ultimate Focus mode enabled. Slides were kept at 37°C within the environmental control unit enclosing the microscope stage. Images were deconvolved in DeltaVision SoftWoRx (version 6.5.2). Figure panels were created in Adobe Photoshop (21.2.0) and Adobe Illustrator (24.2).

Quantification and analysis of fluorescence and time-lapse microscopy data.

All quantification of fluorescence microscopy and time-lapse microscopy data was performed on non-deconvolved DeltaVision image files (opened as TIFFs) in FIJI version 2.3.0/1.53q. All images were automatically scaled appropriately depending on the individual DeltaVision Elite Deconvolution microscope used for data collection. All cells that were in focus and fully within a field were analyzed for each image. To obtain a representative sample, n > 150 when possible. The cross-sectional area and DAPI intensity of phage DNA (intra- or extracellular) were measured using the FIJI

freehand selection tool at the point in the z-series in which the measured object was in focus. If a cell was infected multiple times (indicated by multiple distinct foci of phage DNA or mature phage nuclei), the phage DNA with the greatest cross-sectional area was measured. Data was analyzed and figures were generated using Microsoft Excel (version 16.75.2) and Python 3.

Percentage of phage nuclei that colocalize with sfGFP-ChmA during ChmA knockdown was determined via manual inspection of GFP and DAPI channels. Data analysis was performed in Microsoft Excel (version 16.75.2).

For time-lapse microscopy, each cell visibly swollen or containing a phage nucleus was tracked over 210 minutes. The data was analyzed and final figure generation was performed in GraphPad Prism (version 10.0.0 (131)).

In situ Cryo-EM sample preparation and data collection.

For grid preparation of Goslar infected cells, 10 µL of OD_{600} 0.4 cells were spread on ten 1% agarose, 25% LB pads plates containing 30 µg/mL chloramphenicol and 5 nM aTc. After incubating at 37°C for 2 hours, cells were infected with 10 µL ~10^{10} PFU/mL Goslar lysate and incubated again at 37°C. 90 mpi, cells were collected by the addition of 25 µL of 25% LB to each pad and gentle scraping with the bottom of an Eppendorf tube followed by aspiration.

A volume of 4µl of cells was deposited on R2/1 Cu 200 grids (Quantifoil) that had been glow-discharged for 1 min at 0.19 mbar and 20 mA in a PELCO easiGlow device shortly before use. Grids were mounted in a custom-built manual plunging device (Max Planck Institute of Biochemistry) and excess liquid blotted with filter paper (Whatman no. 1) from the backside of the grid for 5–7 s prior to freezing in a 50:50 ethane:propane mixture (Airgas) cooled by liquid nitrogen.

Grids were mounted into modified Autogrids (Thermo Fisher Scientific) compatible with cryo-focused ion-beam (cryo-FIB) milling. Samples were loaded into an Aquilos 2 dual beam microscope (TFS) and milled to generate lamellae approximately ~150–250 nm thick as previously described (31).

Cryo-EM data was collected on a Titan Krios G3 (Thermo Fisher Scientific) operated at 300 keV equipped with a K3 detector and 1067HD BioContinuum energy filter (Gatan) with 15 eV slit-width. Tilt series were acquired at a pixel sizes of 1.62 and 3.22 Å/pixel with tilt range of +/- 54° and 3° increments starting from a lamella pre-tilt of 9-12° using the dose-symmetric scheme. Data was acquired automatically using SerialEM v4.1-beta (32) with parallel cryo electron tomography (PACE-tomo) scripts (33) and a 4 µm nominal defocus. The first projection of each tilt series was collected with a ~20 e-/Å fluence and the remaining tilts at ~3.6 e-/Å /tilt, giving a total fluence of 140 e/Å. All tilt series were processed and reconstructed into tomograms using Warp v1.1.0-beta (34), with whole-frame tilt series alignment performed in AreTomo v1.3.3 (35).

In situ Cryo-EM analysis of EPI vesicles and ribosomes.

EPI vesicles and phage nuclei were manually counted from montages acquired at 7.62 nm/px prior to collection of tilt series. Membrane segmentations were generated from deconvolved tomograms using membrain-seg v1 and the pre-trained model v10 from the developers (36). To measure the diameters of EPI vesicles, each vesicle was manually defined by a set of points in the deconvolved tomogram in IMOD (37) to create a point cloud. Because most EPI vesicles were not fully contained within the tomogram due to FIB milling of the sample, the diameter of the EPI vesicles were estimated by using a least-squares fit of the point cloud to a sphere function (38). Sphere diameter measurements were performed at both magnifications and combined.

Ribosomes were detected using the crYOLO deep-learning particle-picker in tomography mode (39), yielding 7050 and 22371 particles from the 1.62 and 3.22 Å/px datasets across 10 and 11 tomograms, respectively. Each dataset was trained separately using manually picked ribosomes from 13 slices of a single representative tomogram in the 1.62 Å/px dataset and 10 slices across two representative tomograms for the 3.22 Å/px dataset. Subtomograms from both datasets were reconstructed at 10 Å/px using Warp and refined to convergence using RELION v3.1 (40). To ensure more accurate diameter measurements, pixel sizes were calibrated from these ribosome averages using a high-resolution cryo-EM structure (PDB 7K00) fitted into the density at a range of pixel sizes.

As it appeared visually that polysomes were present in the periphery of EPI vesicles, we set out to identify polysomes quantitatively. To identify chains of translating ribosomes, disomes from obvious polysomes were selected to define a relative rotation based on known orientations from subtomogram refinements at 10 Å/px. A pairwise search for disomes conforming to this relationship was conducted using ribosomes with less than 30 nm inter-particle spacing – slightly larger than a 70S ribosome diameter – thereby generating a list of conforming pairs. Chains were identified from this using group theory implemented with NetworkX functions (41). Scenes depicting ribosomes and membrane segmentations were rendered in ChimeraX (42) with the ArtiaX plug-in (43).

Sample Preparation for Mass Spectrometry.

200 µL of OD_{600} 0.2 cells were spread on 1% agarose, 25% LB, 6 cm diameter plates containing 30 ug/mL chloramphenicol and 5 nM aTc. After incubating at 37°C for 2 hours, cells were infected with 100 µL ~10^{10} PFU/mL Goslar lysate and incubated again at 37°C. 30 mpi, cells were collected in 1 mL 25% LB and centrifuged at 1500 x g at 4°C and washed three times to remove phage particles. Cell pellets were stored at -80°C. All samples were prepared as biological triplicate. Frozen cell pellets (200 µL) were thawed on ice and resuspended with 200 µL water to give a volume of 400 µL. 10 µL of resuspended cells were mixed with 200 µL of 6M guanidine-HCl, vortexed, then incubated 3 times at 100°C for 5 minutes, followed by cooling to room temperature. 1.8 mL pure methanol was added to each lysate, the mixture was briefly vortexed, then incubated at -20°C for 20 minutes. Following incubation, samples were centrifuged at 18000 x g for 10 minutes at 4°C and the supernatant was removed. The pellet was resuspended in 200 µL of 8 M urea in 0.2 M ammonium bicarbonate and incubated for one hour at 37°C with constant agitation. After incubation, 4 µL of 500 mM TCEP (Tris(2-carboxyethyl) phosphine) and 20 µL 400 mM chloro-acetamide were added to each sample. Protein concentration was measured by BCA assay, then 600 µL of 200 mM ammonium bicarbonate was added, bringing the urea concentration to 2 M. Sequencing grade trypsin was added to each sample at 1 µg for each 100 µg of protein in the sample, and mixtures were incubated overnight at 42°C. 50 µL of 50% formic acid was then added, bringing the pH to 2. Samples were desalted using C18 solid phase extraction (Waters Sep-Pak C18 12 cc Vac Cartridge, WAT036915) according to the manufacturer protocol. The final protein concentration of each sample was measured using BCA after resuspension in 1 ml PBS.

LC-MS-MS.

The peptides of each sample were analyzed by ultra-high pressure liquid chromatography coupled with tandem mass spectrometry using nano-spray ionization with an Orbitrap Fusion Lumos hybrid mass spectrometer (Thermo Fisher Scientific) interfaced with a nano-scale reversed-phase UPLC (Thermo Fisher Scientific Dionex UltiMate 3000 RSLCnano System) fitted with a 25 cm, 75-micron ID glass capillary packed with 1.7-µm C18 (130) BEH beads (Waters). Peptides were eluted from the C18 column to the mass spectrometer using a linear gradient of 5–80% acetonitrile (ACN) at a flow rate of 375 µL/min for 3 hours. The ACN gradient was created with these buffers: Buffer A (98% H2O, 2% ACN, 0.1% formic acid) and Buffer B (100% ACN, 0.1% formic acid).

The parameters for the mass spectrometer were as follows: MS1 survey scan using the Orbitrap detector (mass range (m/z): 400-1500 (using quadrupole isolation), 120000 resolution setting, spray voltage 2200 V, ion transfer tube temperature 275°C automatic gain control (AGC) target value 400000, and maximum injection time of 50 ms), followed by MS2 data dependent scans (top speed for most intense ions, with charge state set to only include +2-5 ions, and 5 second exclusion time). Ions were selected with minimal intensities of 50,000 when the collision was carried out in a high energy collision cell (30% HCD Collision Energy). The fragment masses were analyzed in the ion trap mass analyzer, with ion trap scan rate of turbo (first mass m/z 100, AGC Target 5000, and maximum injection time of 35 ms). Protein identification and label free quantification was carried out using Peaks Studio 8.5 (Bioinformatics Solutions Inc.)

Mass Spectrometry Analysis.

For each sample, peptides identified by mass spectrometry were divided into host (*E. coli* MC1000, using the *E. coli* MG1655 proteome) and phage (Goslar) peptides. For normalization, common OmpA peptides that were detected in all runs were sorted and the sum of common OmpA peptides'

peak areas were used as the normalization coefficient for the corresponding run. Normalized peak areas of Goslar proteins were calculated for each sample (biological triplicate). Student's T-Test was used to compare the average peak areas of each Goslar protein detected in the non-targeting versus knockdown host strain. The twenty phage proteins detected in each replicate and with the greatest average normalized peak area in the non-targeting strain samples are displayed in **Fig. 5A**. Peak areas of all detected Goslar proteins are provided in **Table S1**.